Journal of
Cerebral Blood Flow
& Metabolism

Signal separation and parameter estimation in non-invasive dual-tracer PET scans using reference region approaches

Journal:	*Journal of Cerebral Blood Flow and Metabolism*
Manuscript ID:	JCBFM-0528-08-ORIG.R1
Manuscript Type:	Original Articles
Date Submitted by the Author:	
Complete List of Authors:	Joshi, Aniket; University of Michigan, Department of Biomedical Engineering Koeppe, Robert; University of Michigan, Radiology (Nuclear Medicine) Fessler, Jeffrey; University of Michigan, Department of Electrical Engineering and Computer Science Kilbourn, Michael; University of Michigan, Radiology (Nuclear Medicine)
Keywords:	PET (positron emission tomography), reference regions, tracer kinetic modelling < kinetic modeling, brain imaging < imaging

Signal separation and parameter estimation in non-invasive dual-tracer PET scans using reference region approaches

Aniket D. Joshi[1,3], Robert A. Koeppe[1], Jeffrey A. Fessler[1,2,3], Michael R. Kilbourn[1]. [1]Division of Nuclear Medicine, Department of Radiology, University of Michigan, Ann Arbor, MI; [2]Electrical Engineering and Computer Science, College of Engineering, University of Michigan, Ann Arbor, MI; [3]Biomedical Engineering, College of Engineering, University of Michigan, Ann Arbor, MI.

Corresponding Author

Robert A. Koeppe

University of Michigan

Department of Radiology

Division of Nuclear Medicine

3480 Kresge III 0552

Ann Arbor, MI 48109-0552

Telephone: (734) 763-9247

Telefax: (734) 764-0288

e-mail: koeppe@umich.edu

Running Title: Non-invasive dual-tracer PET: Human studies

ABSTRACT

This is the first study to report results from non-invasive dual-tracer PET in humans not requiring arterial sampling, where two radiotracers were injected closely in time within the same scan. These studies yield near simultaneous information on two different neuropharmacological systems, providing better characterization of a subject's neurological condition. The non-invasive dual-tracer approach described here is based on the primary assumption that an appropriate bolus+constant infusion protocol brings the reference tissue of the first radiotracer to steady state prior to injection of the second tracer. Two methods for separation of time-activity curves (TACs) and parameter estimation were investigated: i) an extrapolation method where first tracer's TACs were extrapolated over total scan duration followed by subtraction from dual-tracer TACs and ii) a simultaneous fitting method where reference region models for both tracers were fitted simultaneously to dual-tracer TACs. Combinations of two reversible tracers ([^{11}C]flumazenil and [^{11}C]dihydrotetrabenazine) or one reversible and one irreversible tracer ([^{11}C]N-methylpiperidinyl propionate) were used. Following the dual-tracer scan, a single-tracer scan using one of the tracers was obtained for comparison of the dual-tracer results. Both approaches provided parameter estimates with inter-subject regions-of-interest means typically within 10% of those obtained from single-tracer scans without an appreciable increase in variance.

INTRODUCTION

Dual-tracer PET methodology provides an opportunity to characterize two different neuropharmacological aspects of a subject from a single PET acquisition. Typically, measurement of two different pharmacological aspects using PET would involve two separate single-tracer PET scans. The dual-tracer methodology can obtain data related to two systems-of-interest almost simultaneously by injecting two tracers separated closely in time within a single PET scan. Dual-tracer PET data analysis presents a challenge as all positron emitting isotopes emit photons with 511 KeV energy and it is not possible to separate the signals from the two tracers using differing energy windows. Injecting two tracers simultaneously would make it impossible to separate the two signals; hence tracer injections in this work were staggered in time by 20 or 30 min.

The earliest work in dual-tracer PET was done in phantom studies where differences in tracer half-lives were used for signal separation (Huang et al. 1982). Koeppe et al. 2001 reported the first results of dual-tracer brain PET studies in humans using ^{11}C labeled tracers where tracer models were fitted simultaneously to estimate the parameters of both tracers using metabolite-corrected arterial plasma input functions. Kadrmas and Rust (2005) evaluated the possibility of a similar parallel-model fitting approach in a simulation study for rapid dual-tracer scans. Various applications of rapid dual-tracer studies have been described recently including simulation studies for measuring hypoxia and blood flow (Rust and Kadrmas 2006) and tumor characterization using ^{62}Cu-PTSM and ^{62}Cu-ATSM in dogs (Black et al. 2008).

The existing work on dual-tracer studies mentioned above is based on an arterial sampling approach, which is inconvenient for the subjects due to its invasive nature and difficult due to the requirement of plasma metabolite correction for each of the two tracers. This paper

reports results of a new non-invasive, dual-tracer brain PET approach in humans that is based on a reference tissue model instead of an arterial plasma input function model.

The possibility of analysis of dual-tracer studies without arterial sampling was first explored in Koeppe et al. (2004). In the present paper, we have extended this original work and report two reference tissue methods for separating the individual tracer signals and estimating parameters of interest: i) an extrapolation method (EM) where first tracer's TACs were extrapolated over total scan duration followed by subtraction from dual-tracer TACs and ii) a simultaneous fitting method (SM) where reference region models for both tracers were fitted simultaneously to dual-tracer TACs. The pharmacological indices of interest in the dual-tracer studies were the blood-brain barrier transport parameter (R_1), distribution volume ratio for reversible tracers (DVR= BP_{ND}+1, where BP_{ND} is the non displaceable binding potential (Innis et al. 2007)), and k_3 (the trapping constant), for irreversible tracers.

In this work, we have attempted to minimize the variance in the parametric images by implementing the following three steps: a) noise reduction in TACs by an adaptive smoothing approach, b) reduction in the number of parameters to be fitted by fixing the k_4 parameter for both tracers to their population average in the full reference tissue model for reversible tracers (Cunningham et al. 1991; Lammertsma et al. 1996), and c) application of robust linear estimation techniques such as Logan analysis to single-tracer curves extracted from dual-tracer data. Each of these steps are described in detail in the methods section.

The dual-tracer scans were also followed by single-tracer scan of one of the tracers to provide a 'gold standard' for comparison of dual-tracer results. The parametric images obtained from dual tracer studies were in good agreement with the single tracer studies with similar noise properties and inter-subject regions-of-interest means typically within 10%.

METHODS

Radiotracers:

The radiotracers used in this study have been well characterized for traditional single-tracer PET scans at our institution: flumazenil ([^{11}C]FMZ), a benzodiazepine receptor antagonist (Holthoff et al. 1991; Koeppe et al. 1991); dihydrotetrabenazine ([^{11}C]DTBZ), a ligand for the VMAT2 binding site (Koeppe et al. 1999a; Koeppe et al. 1997; Koeppe et al. 1996); and N-methylpiperidinyl propionate ([^{11}C]PMP), a substrate for hydrolysis by the enzyme acetylcholinesterase (Koeppe et al. 1999b). Both [^{11}C]FMZ and [^{11}C]DTBZ can be classified as reversible tracers and have been analyzed successfully using both bolus and bolus+continuous infusion protocols (Frey et al. 1993; Koeppe et al. 1997). [^{11}C]PMP can be classified as an irreversible tracer.

Key assumption:

The key assumption in non-invasive dual-tracer PET is that an appropriate bolus plus constant infusion protocol for the first tracer brings its reference region to steady state prior to the injection of the second tracer. Simply put, the fate of the first tracer's reference region is assumed to be known since its concentration is constant from the time the second tracer is injected until the end of the scan despite "contamination" by the second tracer (Koeppe et al. 2004). The more rapidly reversible a tracer is, the more likely for this key assumption to hold true.

Data acquisition, reconstruction, and processing:

Dual-tracer studies were performed on 37 healthy subjects using the following two tracer pairs: (1) [^{11}C]FMZ and [^{11}C]DTBZ, or (2) [^{11}C]FMZ and [^{11}C]PMP. Table 1 summarizes the details such as order in which the tracers were injected, the time difference between tracer

injections, and the single-tracer scan that followed the dual-tracer scan. The irreversible tracer [^{11}C]PMP has no region of negligible trapping; thus, only [^{11}C]FMZ and [^{11}C]DTBZ, with pons and occipital cortex as reference regions respectively, were used as the first tracers in this work, while [^{11}C]PMP was used exclusively as a second tracer. For studies in which [^{11}C]FMZ was injected first, studies were performed with two delay windows between tracer injections (20 and 30 min). It was not possible to reliably achieve steady state in the occipital cortex, the reference tissue for [^{11}C]DTBZ, by 20 minutes. Hence studies where [^{11}C]DTBZ was injected first were performed with a 30 min injection offset. The injected radioactivities were approximately the same for both tracers. Twelve mCi (444 MBq) ±10% of each tracer was administered. Scan data was acquired for 80 min as a dynamic sequence of 26 or 27 frames for 20 or 30 min offsets, respectively. The dual-tracer studies were followed by a 60 min single-tracer scan using one of the tracers used in the dual-tracer study. Each single-tracer scan provided a 'gold standard' for comparison with one of the tracers from the dual-tracer scan. Single tracer studies were not performed for both the dual-scan tracers due to time and dosimetry constraints. The single-tracer scans were also used to assess the validity of the key assumption that the first tracer's reference tissue reaches steady-state before the second tracer is administered.

All PET scans were acquired in 3-D mode on an ECAT EXACT HR+ tomograph (Siemens Medical Systems, Inc., Knoxville, TN, USA). Images were reconstructed using Fourier rebinning (FORE) (Defrise M et al. 1997) of the 3-D data into 2-D sinograms and ordered subsets expectation maximization (OSEM) (Comtat et al. 1998; Hudson and Larkin 1994) using 4 iterations and 16 subsets.

Subject motion across frames was corrected using Neurostat, initially developed at the University of Michigan (Minoshima et al. 1994; Minoshima et al. 1993). Scans were reoriented

to the stereotactic atlas of (Talairach and Tournoux 1988), followed by both linear scaling and non-linear warping.

All modeling estimations were performed voxel-by-voxel, creating parametric images of the BBB transport parameter (R_1), the distribution volume ratio (DVR = $1+BP_{ND}$; (Innis et al. 2007)) for the reversible tracers, and a 'trapping rate' parameter (k_3) for the irreversible tracer. Volumes-of-interest (VOIs) were obtained using a standardized VOI template defined in Talairach atlas space.

Dual-tracer signal separation techniques:

The proposed reference tissue-based dual-tracer approach is suitable for cases where the first tracer injected has a tissue or a region with negligible receptor binding or trapping. We first describe the methods for the case where both injected radiotracers bind reversibly and then extend it to the case where the first tracer has reversible binding and the second tracer has irreversible trapping.

In the case of a reversible single-tracer two-tissue compartment model, the target region concentration time courses or time-activity curves (TACs) can be expressed in terms of the model rate constants and reference region concentration time course using the full reference tissue input model equation shown in equation (1) below (Cunningham et al. 1991; Lammertsma et al. 1996):

$$y_i(t) = R_1\left(y_r(t) + ay_r(t) \otimes e^{-ct} + by_r(t) \otimes e^{-dt}\right), \quad (1)$$

where, $y_i(t)$ is the target region concentration time course for region or voxel *i*, $y_r(t)$ is the reference region concentration time course and *R, a, b, c* and *d* are model parameters that are functions of the rate constants of a two tissue compartment model: $K_1 - k_4$ and K_1^{ref} ($K_1 - k_4$ are

the rate constants of a two tissue compartment model and K_1^{ref} is the transport parameter for the reference region). PET TACs are obtained by binning the instantaneous PET data over N temporal frames. The target region TAC binned into N temporal frames can be enumerated for voxel i as $\bar{y}_i = [y_i^1 ... y_i^N]$, where $y_i^j = \frac{1}{t_{end}^j - t_{start}^j} \int_{t_{start}^j}^{t_{end}^j} y_i(t)dt$ and t_{start}^j and t_{end}^j are the start and end times of the j^{th} frame. The reference region TAC vector $\bar{y}_r$ can also be obtained similarly. The model parameters can be arranged in a parameter vector form as follows:

$$\bar{\theta}_i = [\frac{K_1}{K_1^{ref}}, k_2, k_3, BP_{\text{ND}}]_i, \quad (2)$$

where $BP_{\text{ND}} = \frac{k_3}{k_4}$. Using equations (1) and (2), we can express the TAC ($\bar{y}_i$) as a function of the reference region TAC ($\bar{y}_r$) and the parameter vector ($\bar{\theta}_i$) plus a residual error term ($\bar{\varepsilon}_i$) as shown below.

$$\bar{y}_i = f(\bar{y}_r, \bar{\theta}_i) + \bar{\varepsilon}_i \ . \quad (3)$$

The parameter vector can be estimated using nonlinear least-squares to minimize the difference between the model-predicted and measured data:

$$\hat{\bar{\theta}}_i = \arg\min_{\theta_i} \left\| \bar{y}_i - Wf(\bar{y}_r, \bar{\theta}_i) \right\|_2^2. \quad (4)$$

where, W is the weighting matrix that takes into account the difference in variance between different frames of the PET scan. The normalized variance for the j^{th} frame is given by $\sigma_j^2 = \frac{y_i^j e^{\lambda T_j}}{t_{end}^j - t_{start}^j}$ (Logan et al. 2001) where T_j is the midpoint time for the j^{th} frame and λ is the

known tracer decay constant (λ = 0.0347 min^{-1} for ^{11}C tracers). The weighting matrix $W \in R^{N\times N}$ is a diagonal matrix with $\frac{1}{\sigma_j^2}$ along the diagonal (Faraway 2004).

The above equations (1 - 4) are derived for a single tracer. In a dual-tracer study, two tracers are injected; Tracer *II* injected at time $t = T'$ after Tracer *I*. The dual-tracer TAC ($\bar{y}_i$) can be represented as:

$$\bar{y}_i = \bar{y}_i^I + \bar{y}_i^{II} + \bar{\varepsilon}_i, \quad (5)$$

where $\bar{y}_i^I$ and $\bar{y}_i^{II}$ are the constituent individual tracer signals and $\bar{\varepsilon}_i$ is the noise vector.

The present work investigated two methods to estimate the individual tracer curves ($\bar{y}_i^I$ and $\bar{y}_i^{II}$) and their parameter vectors ($\bar{\theta}_i^I$ and $\bar{\theta}_i^I$) from the dual-tracer signal $\bar{y}_i$: an extrapolation method (EM) and a simultaneous fitting method (SM).

1. Extrapolation Method (EM)

The extrapolation method is based on the original approach reported in Koeppe et al. (2004), where the simplified reference tissue model (sRTM; Lammertsma and Hume 1996) was used to extrapolate the first tracer, while in this case we use the full reference tissue model. Data exclusive to Tracer *I* is known for $t < T'$; the injection time of Tracer *II*. Using this early data, Tracer *I* parameter vector for each voxel *i* ($\bar{\theta}_i^I$) could be estimated by minimizing the cost function shown below using some nonlinear estimation algorithm.

$$\hat{\bar{\theta}}_i^I = \arg\min_{\bar{\theta}_i^I} \left\| \bar{y}_i^I - Wf(\bar{y}_r^I, \bar{\theta}_i^I) \right\|_2^2 \quad (6)$$

However, this minimization required nonlinear estimation of the four parameters from just 20 min of data which gave noisy estimates. To counter this problem, the parameter-of-interests, R_1

($\frac{K_1}{K_1^{ref}}$) and DVR (=1+BP_{ND}) for Tracer *I*, were first estimated by the using PCA-based reference-region Logan plot analysis (Joshi et al. 2008) from the first 20 min. The remaining unknown elements of the parameter vector $\overline{\theta}_i^I$ (k_2, k_4) were estimated using nonlinear least squares from equation (6). Using this parameter vector and the reference region TAC for Tracer *I*, Tracer *I* TACs were extrapolated till the end of scan duration using the full reference tissue model ($\hat{\overline{y}}_i^I = f(\overline{y}_r^I, \hat{\overline{\theta}}_i^I)$). Tracer *II* component was isolated by subtracting the extrapolated Tracer *I* signal from the dual-tracer TAC for all voxels *i* ($\hat{\overline{y}}_i^{II} = \overline{y}_i - \hat{\overline{y}}_i^I$). The isolated Tracer *II* curves ($\hat{\overline{y}}_i^{II}$) also include the reference region curve for Tracer *II* ($\hat{\overline{y}}_r^{II}$) and hence, all the information to estimate the parameter-of-interest for Tracer *II* (DVR and R_1) using PCA-based Logan analysis has been obtained.

2. Simultaneous Fitting Method (SM)

A potential drawback of the two-step extrapolation method described above is that errors in parameter estimation of Tracer *I* from limited early data propagate into parameter estimates of Tracer *II*. There may be cases where error in Tracer *I* estimates could propagate in such a way to give physiologically improbable parameter values for Tracer *II*. Thus, as an alternative to the two-step extrapolation method, we also explored a one step approach where the parameters of both the tracers were estimated at the same time by fitting the dual tracer TACs to the reference tissue models of both tracers simultaneously.

This simultaneous fitting method (SM) attempted to estimate the model parameters for both tracers using one minimization operation. We first applied the extrapolation method to the dual-tracer curve of Tracer *II* reference region alone, to isolate Tracer *II* reference region curve

($\hat{\bar{y}}_r^{II}$). Tracer *I* reference region TAC ($\bar{y}_r^{I}$) was known by virtue of the primary assumption. Using the reference region curves for both tracers, the voxel-wise parameter vectors for both the tracers could be estimated simultaneously by minimizing the following cost function:

$$(\hat{\bar{\theta}}_i^{I}, \hat{\bar{\theta}}_i^{II}) = \underset{(\bar{\theta}_i^{I}, \bar{\theta}_i^{II})}{\arg\min} \left\| \bar{y}_i - W\{f(\bar{y}_r^{I}, \bar{\theta}_i^{I}) + f(\hat{\bar{y}}_r^{II}, \bar{\theta}_i^{II})\} \right\|_2^2. \quad (7)$$

The primary parameter-of-interest (DVR) for both tracers could now be calculated directly from the estimated parameter vectors $\hat{\bar{\theta}}_i^{I}$ and $\hat{\bar{\theta}}_i^{II}$.

Using an irreversible tracer as Tracer *II*

The methods described above were for the case where both the tracers injected bind reversibly, though they can easily be extended to the case where Tracer *II* has irreversible kinetics. However in the case of an irreversible tracer, the reference region-based model equations for the TACs will be different from that for a reversible tracer (equation (1)).

The differential equations for an irreversible two-tissue compartment model are given below ($k_4^{II} = 0$ in Figure 1):

$$\frac{dC_{\mathrm{ND}}(t)}{dt} = K_1 C_p(t) - (k_2 + k_3) C_{\mathrm{ND}}(t), \quad (8)$$

$$\frac{dC_{\mathrm{S}}(t)}{dt} = k_3 C_{\mathrm{ND}}(t), \quad (9)$$

where $C_p(t)$ is the arterial plasma input, $C_{\mathrm{ND}}(t)$ is the radioligand concentration in the non-displaceable compartment, $C_{\mathrm{S}}(t)$ is the radioligand concentration in the specific compartment, and K_1, k_2, and k_3 are the kinetic parameters of the model with k_3, the trapping constant, being the parameter of interest to be estimated from the dynamic data. In case of the arterial sampling

approach, the solution for total tracer concentration in tissue ($y_i = C_{ND} + C_S$) is given below (Herholz et al. 2001):

$$y_i(t) = \frac{K_1 k_2}{k_2 + k_3} \int_0^t C_p(\tau) e^{-(k_2+k_3)(t-\tau)} d\tau + \frac{K_1 k_3}{k_2 + k_3} \int_0^t C_p(\tau) d\tau, \quad (10)$$

where $C_p(\tau)$ denotes the arterial input function. For the case of an irreversible tracer like [^{11}C]PMP, the basis for the reference tissue approach is not that the reference tissue is void of specific uptake, but in fact the opposite, that the reference tissue has such a high rate of irreversible trapping that all tracer that enters the reference tissue is trapped and none clears back into the blood. Thus, we assume that the TAC of the reference tissue, which is the basal ganglia for [^{11}C]PMP, is proportional to the integral of the arterial input function. Kinetic studies of [^{11}C]PMP indicate that only about 10% of the tracer entering the basal ganglia clears back to tissue, while about 90% is irreversibly trapped (Koeppe et al. 1999b).

The irreversible tracer TAC from a region with an extremely high k_3 value (e.g. striatum for [^{11}C]PMP) is assumed to equal the time integral of the arterial input function multiplied by the transport rate constant of the reference region, K_1^{ref} (Herholz et al. 2001; Nagatsuka et al. 2001):

$$y_r(t) = K_1^{ref} \int_0^t C_p(\tau) d\tau. \quad (11)$$

Equation (11) was rearranged to get an expression for the plasma input function in terms of the reference region curve as shown below:

$$C_p(t) = \frac{1}{K_1^{ref}} \frac{dy_r(t)}{dt}. \quad (12)$$

The differentiation operation in equation (12) was performed by interpolating the reference region curve on a fine grid followed by numerical differentiation. Substituting the expression for $C_p(t)$ obtained from equation (12) in equation (10) yielded:

$$y_i(t) = (\frac{K_1}{K_1^{ref}})\frac{k_2}{k_2+k_3}\int_0^t \frac{dy_r(\tau)}{d\tau} e^{-(k_2+k_3)(t-\tau)} d\tau + (\frac{K_1}{K_1^{ref}})\frac{k_3}{k_2+k_3} y_r(t), \quad (13)$$

which expresses the target tissue curve in terms of the reference tissue curve and the rate parameters for irreversible tracers and is equivalent to equation (1) for reversible tracers.

Using the notation derived for reversible tracers, the TAC for an irreversible tracer can be expressed as $\overline{y}_i = f(\overline{y}_r, \overline{\theta}_i) + \overline{\varepsilon}_i$, where $\overline{y}_i$ is the tissue TAC, $\overline{y}_r$ is the reference region curve, $\overline{\theta}_i = [\frac{K_1}{K_1^{ref}}, k_2, k_3]$ is the parameter vector for irreversible tracers and the function *f* is reference tissue model in equation (13).

After signal separation, the parameter of interest for the irreversible tracer (k_3) was estimated by the reference-region based linear least squares method (RLS) as proposed in (Nagatsuka et al. 2001). The operational equation of RLS is shown below.

$$\overline{y}_i(T) = \rho_1 \overline{y}_r(T) + \rho_2 \int_0^T \overline{y}_r(\tau) d\tau + \rho_3 \int_0^T \overline{y}_i(\tau) d\tau \quad (14)$$

where ρ_1, ρ_2 and ρ_3 are the coefficients of the linear model above and $k_3 = \rho_2 / \rho_1$.

Robust parameter estimation:

To improve the robustness of the parameters of interest obtained from the non-invasive dual-tracer PET, the following three procedures were developed and implemented:

Adaptive smoothing:

In this step, a spatially dependent smoothing protocol was implemented to reduce noise in TACs prior to the signal separation and parameter estimation steps. The neighborhood of the voxel's TAC under consideration (y_i) was searched to identify those TACs that had shapes similar to that of y_i. An average of the TAC under consideration and the qualifying neighboring TACs yielded a TAC with reduced noise. This approach caused little smoothing in regions with kinetically distinct voxels, thus preserving spatial resolution. The procedure is mathematically represented below:

A set of voxel indices N_i was selected for the voxel i under consideration such that:

$$N_i = \{ j : \left\| y_i - y_j \right\|_2 < T \}, \quad (15)$$

where y_j is the TAC of a neighboring voxel j, $\| y_i - y_j \|_2$ is the L_2-norm of the difference vector between y_i and y_j, and T is the threshold for the L_2-norm and was chosen to be 10% of $\|y_i\|_2$. This threshold was chosen as it gave the best trade-off between noise reduction and preservation of spatial resolution. This search was performed in a 3 x 3 x 3 neighborhood of voxel i. Once such a set TACs was chosen, an average TAC was calculated (y_i^{AVG}) which had less noise than the original dual-tracer TAC (y_i) and was used for curve separation and parameter estimation. This step was applied to both dual-tracer and single tracer scans.

Population average k_4 in the full reference tissue model:

Another step used to improve precision in the separation of the individual tracer components and hence in the binding parameters was reducing the complexity of the full reference tissue model by fixing the k_4 parameter for each tracer to its respective population average value. Our overall goal was the estimation of DVR (=1+BP_{ND}) for each tracer. Since BP_{ND} is equal to the ratio of k_3/k_4, it may seem that using the simplified reference tissue model

where only $1+BP_{ND}$ is estimated instead of k_3 and k_4 separately, would accomplish the same goal. However, the simplifying assumption in sRTM is instantaneous equilibration between free and specific compartments, which implies very high values for both k_3 and k_4. This assumption may bias the shapes of the individual tissue curves for the tracers used in this work. By fixing the k_4 values to the population average values, we reduce the complexity of the full reference tissue model, as in sRTM, but constrain the individual tracer TACs to more closely approximate their true shapes.

Signal separation followed by estimation of binding measures:

For SM, the binding index could be calculated directly from the individual model parameters of the k_4-constrained reference tissue model. However, direct calculation from the individual rate constants may still lack precision despite the adaptive smoothing and k_4 constraint. Instead, the reference tissue model fits to the dual-tracer data (Equation 12) were used only to extract the voxel-wise TAC components for each of the two radiotracers. These separated TACs were then used with robust linear estimation methods to obtain final parametric images (Logan graphical analysis for DVR estimation in reversible tracers and reference-region based linear least squares (RLS) for k_3 estimation in irreversible tracers).

Since the process of signal separation for SM provides smooth TACs, PCA-based Logan analysis is not required and traditional Logan analysis is sufficient. Another point to be noted is that since the parameters-of-interest are estimated after signal separation, the accuracy of the shape of the TAC is of interest, and not the accuracy of the fitted parameter vectors $(\hat{\theta}_i^I, \hat{\theta}_i^{II})$ in Equation 7. The minimization step in equation 7 is an ill-posed problem with multiple solutions, but the shapes of the TACs obtained from each of these solutions of $(\hat{\theta}_i^I, \hat{\theta}_i^{II})$ are nearly identical.

Analysis of single tracer studies:

For the analysis of single tracer studies, adaptive smoothing as described earlier was applied prior to parametric estimation. For reversible tracers, the parameters-of-interest (R_1 and DVR) were estimated using PCA-based Logan plot analysis, and for the irreversible tracer, the parameters-of-interest (R_1 and k_3) were estimated using RLS.

Comparison of dual-tracer and single tracer results:

Parametric estimates of DVR (for FMZ and DTBZ) and k_3 (for PMP) from the two dual-tracers approaches were compared to each other and also to single-tracer estimates using paired Student t-tests. The metric tested was the percent differences between the estimates from different methods for all regions.

RESULTS

Figure 1 shows the average TAC for pons, (reference region for [^{11}C]FMZ) from seven single-tracer [^{11}C]FMZ scan. The pons TAC for each subject has been normalized such that the area under the curve is the same for all subjects. These scans show that it is possible to maintain steady-state in the pons from the time the second tracer has been administered. The infusion protocol (35% bolus-65% infusion) was designed such that steady state was achieved by 20 min, while obtaining reasonable counts in early frames. The error bars indicate standard deviations of the tissue curve values across subjects. A slightly larger standard deviation was seen towards the end of the scan, indicating that some subject's reference tissue TAC may have deviated slightly from steady-state. However, computer simulations have showed that the small deviations from steady state as those seen in Figure 1 are not expected to cause appreciable errors in the estimated parameters (results not shown).

Figure 2 shows the dynamic image sequence from a [^{11}C]FMZ-[^{11}C]DTBZ study where [^{11}C]DTBZ was injected as a bolus 20 minutes after [^{11}C]FMZ. Figure 3 shows the parametric images estimated using EM from a [^{11}C]FMZ-[^{11}C]DTBZ dual-tracer study obtained with the same protocol as shown in Figure 2. The parametric images for both [^{11}C]FMZ (top two rows) and [^{11}C]DTBZ (bottom two rows) are shown for the relative blood brain barrier (BBB) transport rate, R_1 ($=\frac{K_1}{K_1^{ref}}$; rows 1 and 3) and the distribution volume ratio, DVR ($=1+BP_{ND}$; rows 2 and 4).

[^{11}C]FMZ - [^{11}C]DTBZ studies

Figure 4 (panel A) shows distribution volume ratio (DVR) images of three brain slices for studies with the same 20 min FMZ:DTBZ protocol as in Figure 2. The left-most column for each tracer shows the DVR images obtained from a single-tracer scan (ST). The middle and the right-most columns for each tracer show DVR images obtained from the dual-tracer studies using the extrapolation method (EM) and simultaneous fitting method (SM), respectively. Since single-tracer scans were performed using only one of the two tracers used in the dual tracer study, the images seen in the left and right halves of Figure 4 are from different subjects. The dual-tracer scans analyzed using EM and SM yielded images very close in quality to those obtained from single-tracer scans. The image quality tended to improve when the two tracers were separated by 30 min instead of 20 min; since increasing tracer separation improves signal separation as reported for dual-tracer studies using arterial plasma inputs (Koeppe et al. 2001).

The bar graphs in Figure 5 (panel A) show the comparison of the means and standard deviations of eight regions-of-interest extracted from both single-tracer and dual-tracer parametric images. On average, the EM method showed a positive bias in DVR for [^{11}C]FMZ as compared to ST which can be primarily attributed to the fact that 20 min of data was insufficient

to accurately estimate first tracer's transport and binding parameters. As would be expected, the slight positive bias in the DVR estimates of FMZ propagates as a slight negative bias in DTBZ estimates. The magnitude of the DTBZ bias in less pronounced because for this tracer combination, the [^{11}C]DTBZ signal is the dominant contributor to the dual-tracer data (see Figure 2). The inter-subject variance of the dual-tracer methods was only slightly higher on average than those seen in the single-tracer parametric images, indicating that image quality did not suffer due to excessive noise propagation in the dual-tracer approach. Pair-wise t-tests (EM vs. SM, EM vs. ST and SM vs. ST) showed that for the first tracer, EM was significantly higher than SM ($p<0.001$ for all cortical regions), EM was significantly higher than ST ($p<0.05$ in 3 of 4 cortical regions) and there was no significant difference between the SM and ST for all regions ($p=0.15$-0.40). For the second tracer however, no significant difference was seen between the three sets.

[^{11}C]DTBZ - [^{11}C]FMZ studies

Figure 4 (panel B) shows parametric images from studies where [^{11}C]DTBZ was injected first, followed by [^{11}C]FMZ. Again, the dual-tracer methods were successful in accurately separating the individual-tracer signals as indicated by the similarity of ST and either the EM and SM parametric images. Similar to the [^{11}C]FMZ-[^{11}C]DTBZ case, the images for EM method have higher values than those in the single-tracer scan, while the same scan analyzed with the SM method yielded results closer to those of the single-tracer scan.

Figure 5 (panel B) shows trends similar to those seen in panel A, including the positive bias in EM DVR values for the first tracer, which in this protocol was [^{11}C]DTBZ. As before, the inter-subject region-of-interest variance for dual-tracers methods was similar or only slightly higher than those seen in the single-tracer images, again indicating that image quality in dual-

tracer PET is not degraded substantially by propagation of noise. Pair-wise t-tests showed that for first tracer, EM was significantly higher than SM ($p<0.002$ for both caudate nucleus and putamen), and EM values were further away from ST values than those from SM. However, there was no significant difference either between EM and ST or between SM and ST ($p=0.15$-0.35). For the second tracer, there were not significant differences between the three sets.

[^{11}C]FMZ - [^{11}C]PMP studies

Figure 4 (panel C) shows parametric images for a study where [^{11}C]FMZ was injected 30 minutes prior to [^{11}C]PMP. Estimation of the trapping constant for [^{11}C]PMP using the reference-region based linear least squares method (RLS) (Nagatsuka et al. 2001) breaks down in the areas of high trapping due to the ill-conditioned nature of the operational equation (Equation 14). This can be seen in both the single-tracer and dual-tracer k_3 images. AChE activity has a very large dynamic range in the human brain, and since the primary regions of interest for PMP are in the cortex, the images are scaled to better show these values rather than cerebellum (vermis) and brainstem structures which appear as white in the parametric images.

The bar graphs for [^{11}C]FMZ (Figure 5, panel C) showed the familiar features seen in panels A and B: positively biased DVR estimates for EM and a much less pronounced bias for SM-based DVR estimates. The EM-based bias is less for the trapping constant estimation. Estimation of k_3 from signals extracted using SM, on the other hand, is negatively biased in most regions compared to the single-tracer 'gold standard' values. The inter-subject region-of-interest variance for EM and SM was similar to that seen in ST images for [^{11}C]FMZ, but higher for [^{11}C]PMP. For [^{11}C]PMP, the variance in the dual-tracer methods was larger than that in single tracer studies for regions such as thalamus and amygdala that have higher AChE activity. Pair-wise t-tests showed that for the first tracer, EM was significantly higher than SM ($p<0.0002$ for

all cortical regions) and EM values were further away from ST than SM, SM values were not significantly different than ST ($p>0.1$), while EM values were significantly higher than ST ($p<0.005$). For the second tracer, unlike the previous tracer pairs, EM was significantly higher than SM ($p<0.05$ for 3 of 4 cortical regions), while there were no significant differences either EM or SM and ST.

DISCUSSION

This paper presents the first results of human dual-tracer brain PET studies performed non-invasively using reference tissue approaches, hence not requiring arterial blood sampling and plasma metabolite analyses. This non-invasive approach can provide information on two distinct biological systems from a single PET scan. Since the various neurotransmitter systems of the brain do not act in isolation but have complex interactions, dual-tracer methods can be particularly useful in 'challenge' studies where the effect of a pharmacological or behavioral intervention may be on more than a single neuropharmacological system.

The key assumption for this methodology is that the first radiotracer can be brought to steady-state prior to injection of the second radiotracer. This assumption allows one to know the full time course of the reference tissue for the first radiotracer, which acts as the "input function" for the reference tissue model. In general, both reversible and irreversible tracers that satisfy the above criterion could be injected first. In this study however, the irreversible tracer [^{11}C]PMP could not be used first since it has no region that is void of AChE. Rapidly equilibrating tracers, such as flumazenil used here or raclopride, would be expected to work well, while more slowly equilibrating tracers such as methylphenidate or carfentanil, would be poor choices for the "first" tracer.

Of the two analysis approaches evaluated, the extrapolation method, though intuitive, appears to introduce bias in many studies, as parameter estimates derived from only 20-30 min of data can be insufficient for robust parameter estimation. Furthermore, biases in the parameter estimates for the first tracer will propagate as biases in the parameter estimates of the second tracer. The biases in the two tracers, in general, will be negatively correlated, as an error in first tracer's TAC estimation would be compensated by an opposite error in the second tracer's TAC, for the sum of the individual tracer curves to fit the dual-tracer curve. Thus, to avoid the limitations of the EM approach, a simultaneous fitting method was developed and evaluated. In the majority of cases, an improvement of the simultaneous method over EM was seen in terms of better correspondence of the DVR measures with those of the single-tracer scans. This was achieved by fitting the dual-tracer TACs with a combined reference tissue model, to optimally separate the total PET signal into its two 'single-tracer' components. A possible remaining source of bias in the SM approach is that prior to the simultaneous fit, the reference tissue TAC for the second tracer must be determined for which the extrapolation approach was still needed. Once the second reference tissue curve is obtained, the TACs for all voxels can be separated. One aspect of our implementation of the simultaneous method is that after separation of the dual-tracer scan into its individual tracer image sequences, one can redefine the reference-tissue curves on the separated data sets.

One of the primary concerns in any dual-tracer approach is the need to estimate roughly twice as many parameters as compared to a single-tracer PET study. While at first glance, this may seem to be a prohibitive problem, the fact that administration of the two tracers is offset in time provides considerably more 'kinetic' information in a dual-tracer curve than a single tracer curve. However, trying to estimate 6-8 parameters from an 80 min PET session is more challenging that estimating 2-3 parameters from a single-tracer scan, and precision of the

parameter estimates is a concern. Thus, we made efforts along three fronts to enhance precision to provide more robust results.

First, we reduced the voxel-level noise in the TACs by a simple adaptive smoothing procedure. The choice of the threshold for this step must be made carefully, as too high a threshold would result in little smoothing, hence little improvement in precision, while too low a threshold would result in overly degrading the effective spatial resolution of the parametric images. The success of this approach can be seen in the parametric images shown in Figures 3 and 4. In all cases, the apparent noise level is nearly as low for dual-tracer studies as for single-tracer scans.

Second, we fixed the k_4 parameter of the full reference tissue model for both tracers to the population average values during the fitting procedure for separating the dual-tracer signal into its individual components. Using the full reference tissue model (4 parameters, for each tracer), yet fitting only 3 parameters per tracer, helped to stabilize the fit while maintaining a model formulation with more realistic shapes for the tracers' time-activity curves.

Third, while reducing the number of fitted parameters improved the ability to extract the single-tracer curves; using the direct parameter estimates to calculate DVR (=1 + k_3/k_4) with good precision is still limited. This is similar to single-tracer studies, where more stable estimates of DVR can usually be obtained by methods such as Logan plots, rather than directly using nonlinear least squares estimates of individual rate parameters for calculation of DVR. Hence in this study, application of the robust linear Logan graphical analysis was used after separation of individual tracer signals to obtain estimates of the parameters of interest, DVR (RLS for k_3) and R_1. Since the separated tissue time-activity curves were obtained as smooth curves, the potential biases in DVR estimates due to noisy data are avoided.

As expected, increasing the offset in tracer injection time from 20 to 30 minutes provided an improvement in precision for both EM and SM approaches. However, this is a trade-off that would have to be considered for any dual-tracer application. Minimizing the time difference between the administrations of the two tracers would provide more simultaneous estimation of the tracer parameters, but would decrease the precision of parameter estimates. On the other hand, increasing the time difference between tracer injections, while improving precision in parameter estimates, would increase the chance that the biological or pharmacological state of the subject would change. This may be problematic especially in 'challenge' studies where one assumes a variety of biological parameters (blood flow, endogenous neurotransmitter levels, receptor occupancy) are constant over time.

Pair-wise t-tests between the three methods evaluated; single tracer scans (ST) and dual tracer scans analyzed with extrapolation (EM) and simultaneous fitting (SM) methods showed that for the first tracer, SM in general was better than EM and closer to the ST results while for the second tracer the performance of SM and EM was not significantly different that ST.

In conclusion, non-invasive dual-tracer methodology has been shown to produce results comparable to single-tracer scans, and promises to be a very useful technique for nearly simultaneous evaluation of multiple brain systems from a single PET acquisition.

REFERENCES

Black NF, McJames S, Rust TC, Kadrmas DJ. (2008) Evaluation of rapid dual-tracer (62)Cu-PTSM + (62)Cu-ATSM PET in dogs with spontaneously occurring tumors. *Phys Med Biol* 53:217-232

Cunningham VJ, Hume SP, Price GR, Ahier RG, Cremer JE, Jones AK. (1991) Compartmental analysis of diprenorphine binding to opiate receptors in the rat in vivo and its comparison with equilibrium data in vitro. *J Cereb Blood Flow Metab* 11:1-9

Defrise M, Kinihan PE, Townsend DW, Michel C, Sibomana M, DF. N. (1997) Exact and approximate rebinning algorithms for 3-D PET data. *IEEE Trans Med Imaging* 16:145-158

Faraway J. (2004) Weighted Least Squares. In: *Linear Models with R*): CRC Press, pp 92-94

Frey KA, Groom GN, Minoshima S, Koeppe RA, Kuhl DE. (1993) True equilibrium quantification of human cerebral benzodiazepine receptors with the use of [11-C]flumazenil and positron tomography. *J Nucl Med* 34:108P

Herholz K, Lercher M, Wienhard K, Bauer B, Lenz O, Heiss WD. (2001) PET measurement of cerebral acetylcholine esterase activity without blood sampling. *Eur J Nucl Med* 28:472-477

Holthoff VA, Koeppe RA, Frey KA, Paradise AH, Kuhl DE. (1991) Differentiation of radioligand delivery and binding in the brain: validation of a two-compartment model for [11C]flumazenil. *J Cereb Blood Flow Metab* 11:745-752

Huang SC, Carson RE, Hoffman EJ, Kuhl DE, Phelps ME. (1982) An investigation of a double-tracer technique for positron computerized tomography. *J. Nucl. Med.* 23:816-822

Innis RB, Cunningham VJ, Delforge J, Fujita M, Gjedde A, Gunn RN, Holden J, Houle S, Huang SC, Ichise M, Iida H, Ito H, Kimura Y, Koeppe RA, Knudsen GM, Knuuti J, Lammertsma AA, Laruelle M, Logan J, Maguire RP, Mintun MA, Morris ED, Parsey R, Price JC, Slifstein M, Sossi V, Suhara T, Votaw JR, Wong DF, Carson RE. (2007) Consensus nomenclature for in vivo imaging of reversibly binding radioligands. *J Cereb Blood Flow Metab* 27:1533-1539

Joshi AD, Fessler JA, Koeppe RA. (2008) Improving PET receptor binding estimates from Logan plots using principal component analysis. *J Cereb Blood Flow Metab* 28:852-865

Kadrmas DJ, Rust TC. (2005) Feasibility of rapid multitracer PET tumor imaging. *IEEE Trans. Nucl. Imag.* 52:1341-1347

Koeppe RA, Frey KA, Kuhl DE, Kilbourn MR. (1999a) Assessment of extrastriatal vesicular monoamine transporter binding site density using stereoisomers of [11C]dihydrotetrabenazine. *J Cereb Blood Flow Metab* 19:1376-1384

Koeppe RA, Frey KA, Kume A, Albin R, Kilbourn MR, Kuhl DE. (1997) Equilibrium versus compartmental analysis for assessment of the vesicular monoamine transporter using (+)-alpha-[11C]dihydrotetrabenazine (DTBZ) and positron emission tomography. *J Cereb Blood Flow Metab* 17:919-931

Koeppe RA, Frey KA, Snyder SE, Meyer P, Kilbourn MR, Kuhl DE. (1999b) Kinetic modeling of N-[11C]methylpiperidin-4-yl propionate: alternatives for analysis of an irreversible positron emission tomography trace for measurement of acetylcholinesterase activity in human brain. *J Cereb Blood Flow Metab* 19:1150-1163

Koeppe RA, Frey KA, Vander Borght TM, Karlamangla A, Jewett DM, Lee LC, Kilbourn MR, Kuhl DE. (1996) Kinetic evaluation of [11C]dihydrotetrabenazine by dynamic PET:

measurement of vesicular monoamine transporter. *J Cereb Blood Flow Metab* 16:1288-1299

Koeppe RA, Holthoff VA, Frey KA, Kilbourn MR, Kuhl DE. (1991) Compartmental analysis of [11C]flumazenil kinetics for the estimation of ligand transport rate and receptor distribution using positron emission tomography. *J Cereb Blood Flow Metab* 11:735-744

Koeppe RA, Joshi A, Frey K, Snyder SE, Kilbourn MR, Fessler J. (2004) Dual-Tracer PET Studies without Arterial Sampling. *NeuroImage* 22:T115-T116

Koeppe RA, Raffel DM, Snyder SE, Ficaro EP, Kilbourn MR, Kuhl DE. (2001) Dual-[^{11}C]tracer single-acquisition positron emission tomography studies. *J. Cereb. Blood Flow Metab.* 21:1480-1492

Lammertsma AA, Bench CJ, Hume SP, Osman S, Gunn K, Brooks DJ, Frackowiak RS. (1996) Comparison of methods for analysis of clinical [11C]raclopride studies. *J Cereb Blood Flow Metab* 16:42-52

Logan J, Fowler JS, Volkow ND, Ding YS, Wang GJ, Alexoff DL. (2001) A strategy for removing the bias in the graphical analysis method. *J Cereb Blood Flow Metab* 21:307-320

Minoshima S, Koeppe RA, Frey KA, Kuhl DE. (1994) Anatomical standardization: Linear scaling and nonlinear warping of functional brain images. *J Nucl Med* 35:1528-1537

Minoshima S, Koeppe RA, Mintun MA, Berger KL, Taylor SS, Frey KA, Kuhl DE. (1993) Automated detection of the intercommissural (AC-PC) line for stereotactic localization of functional brain images. *J Nucl Med* 34:322-329

Nagatsuka S, Fukushi K, Shinotoh H, Namba H, Iyo M, Tanaka N, Aotsuka A, Ota T, Tanada S, Irie T. (2001) Kinetic analysis of [(11)C]MP4A using a high-radioactivity brain region that represents an integrated input function for measurement of cerebral

acetylcholinesterase activity without arterial blood sampling. *J Cereb Blood Flow Metab* 21:1354-1366

Rust TC, DiBella EV, McGann CJ, Christian PE, Hoffman JM, Kadrmas DJ. (2006) Rapid dual-injection single-scan 13N-ammonia PET for quantification of rest and stress myocardial blood flows. *Phys Med Biol* 51:5347-5362

Rust TC, Kadrmas DJ. (2006) Rapid dual-tracer PTSM+ATSM PET imaging of tumour blood flow and hypoxia: a simulation study. *Phys Med Biol* 51:61-75

Talairach J, Tournoux P. (1988) *Co-planar Stereotaxic Atlas of the Human Brain: 3-Dimensional Proportional System - an Approach to Cerebral Imaging*. New York, NY: Thieme Medical Publishers

Figure Legends

Figure 1: Average time-activity curve (TAC) for pons, the reference tissue for [^{11}C]FMZ, from seven subjects that underwent a 60 min single-tracer [^{11}C]FMZ scan. TACs have been scaled such that the area under the curve is the same for all subjects to account for differences in absolute radioactivity levels. Error bars represent the standard deviation of the TACs for the seven subjects and indicate the degree of variability in maintaining steady-state conditions.

Figure 2: Dynamic dual-tracer PET image sequence for [^{11}C]FMZ - [^{11}C]DTBZ study with a 20 minute offset. The frame sequence for the 80 min scan was four × 0.5 min, three × 1.0 min, two × 2.5 min, two × 5.0 min, (second tracer injected at 20 min), four × 0.5 min, three × 1.0 min, two × 2.5 min, two × 5 min, and four × 10 min frames. The second tracer is injected just before the 12th frame. Note that the much large apparent signal of [^{11}C]DTBZ is in part due to displaying decay corrected data. Hence, the injection of the same dose of [^{11}C]DTBZ at 20 min appeared twice as high relative to the [^{11}C]FMZ in the early frames.

Figure 3: Parametric images obtained from a [^{11}C]FMZ - [^{11}C]DTBZ study at six brain levels. The parametric images shown are R_1, equal to the ratio $\frac{K_1}{K_1^{ref}}$ (rows 1 and 3), and the distribution volume ratio (DVR=1+BP_{ND}) (rows 2 and 4) for both tracers.

Figure 4: Comparison of parametric images of three brain levels from dual-tracer with those from single-tracer studies. The left-most column for each tracer is from a single-tracer study (ST) which acts as 'gold standard' for comparison of dual tracer results. Panel A: [^{11}C]FMZ injected

20 min prior to [^{11}C]DTBZ. Panel B: [^{11}C]DTBZ injected 30 min prior to [^{11}C]FMZ. Panel C: [^{11}C]FMZ injected 30 min prior to [^{11}C]PMP. The extrapolation method (EM) and simultaneous fitting method (SM) show image patterns and magnitudes very close to those from the single tracer (ST) studies.

Figure 5: Comparison of inter-subject means and standard deviations in parametric estimates obtained from single-tracer (ST) and dual-tracer studies analyzed using extrapolation method (EM) and simultaneous fitting method (SM). Results from eight regions-of-interest extracted from parametric images are shown. Panel A: Comparison of dual-tracer [^{11}C]FMZ-[^{11}C]DTBZ studies (n=12) with single tracer studies (n=6). Panel B: Comparison of dual-tracer [^{11}C]DTBZ-[^{11}C]FMZ studies (n=6) with single tracer studies (n=3). Panel C: Comparison of dual-tracer [^{11}C]FMZ-[^{11}C]PMP studies (n=19) with single tracer studies (n=10 for [^{11}C]FMZ and n=9 for [^{11}C]PMP). Error bars represent the standard deviation of the estimated parameters. The regions-of-interest for FMZ are: OCC: occipital cortex, LAT: lateral frontal cortex, SUP: superior parietal cortex, TEM: lateral temporal cortex, CAU: caudate nucleus, THA: thalamus, CER: cerebellar hemisphere, PONS: pons. The regions-of-interest for DTBZ are: PUT: putamen, CAU: caudate nucleus, MID: midbrain, CER: cerebral hemisphere, THA: thalamus, PONS: pons, SUP: superior parietal cortex, OCC: occipital cortex. The regions-of-interest for PMP are: OCC: occipital cortex, LAT: lateral frontal cortex, SUP: superior parietal cortex, TEM: lateral temporal cortex, INS: insular cortex, HIPP: hippocampus, THA: thalamus, AMY: amygdala.

Table 1: Imaging protocol details for dual-tracer studies.

Dual-tracer Scans [a]	Time Difference between tracer injections	Single-tracer scan following the dual-tracer scan	Number of subjects
[^{11}C]FMZ/[^{11}C]DTBZ	20	FMZ	2
		DTBZ	2
		FMZ	1
		DTBZ	1
	30	FMZ	1
		DTBZ	2
		FMZ	2
		DTBZ	1
[^{11}C]DTBZ/[^{11}C]FMZ	30	FMZ	2
		DTBZ	2
		FMZ	1
		DTBZ	1
[^{11}C]FMZ/[^{11}C]PMP	20	FMZ	5
		PMP	5
	30	FMZ	4
		PMP	5

[a] injection order

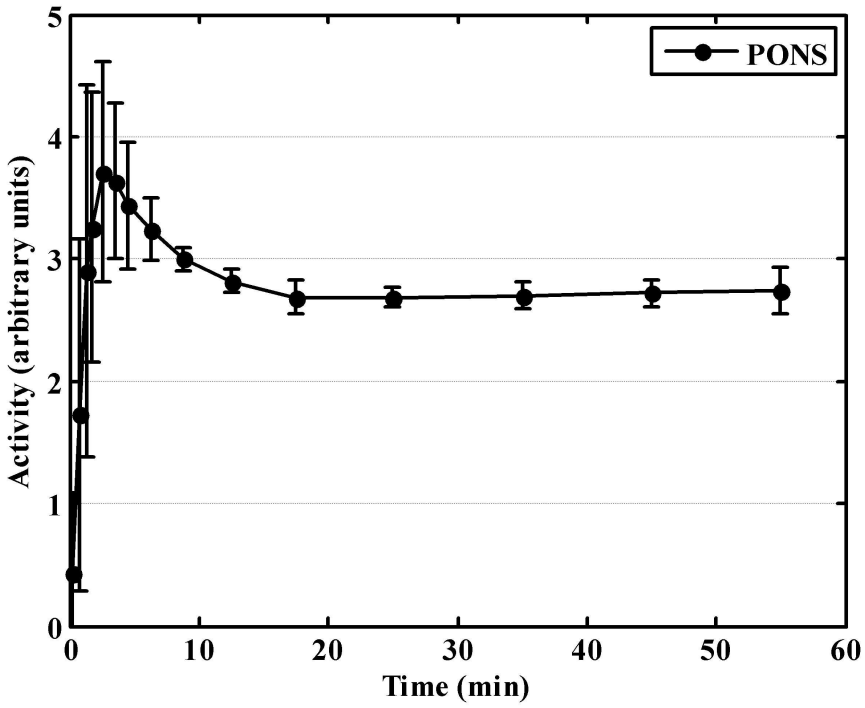

Average time-activity curve (TAC) for pons, the reference tissue for [^{11}C]FMZ, from seven subjects that underwent a 60 min single-tracer [^{11}C]FMZ scan. TACs have been scaled such that the area under the curve is the same for all subjects to account for differences in absolute radioactivity levels. Error bars represent the standard deviation of the TACs for the seven subjects and indicate the degree of variability in maintaining steady-state conditions.
175x131mm (400 x 400 DPI)

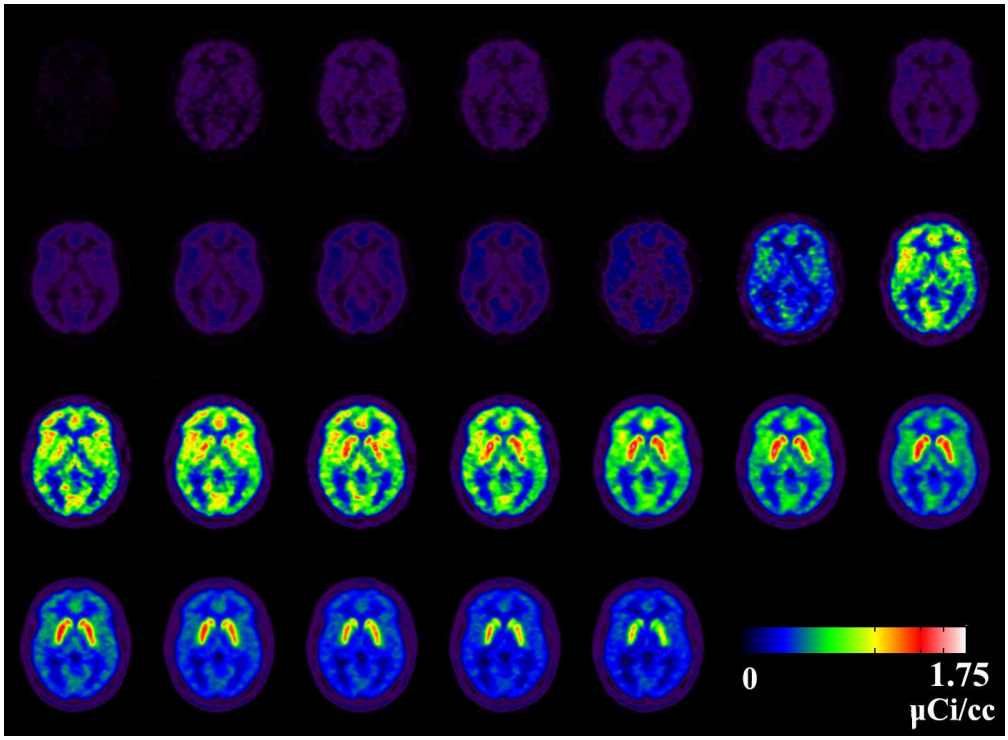

Dynamic dual-tracer PET image sequence for [^{11}C]FMZ - [^{11}C]DTBZ study with a 20 minute offset. The frame sequence for the 80 min scan was four × 0.5 min, three × 1.0 min, two × 2.5 min, two × 5.0 min, (second tracer injected at 20 min), four × 0.5 min, three × 1.0 min, two × 2.5 min, two × 5 min, and four × 10 min frames. The second tracer is injected just before the 12th frame. Note that the much large apparent signal of [^{11}C]DTBZ is in part due to displaying decay corrected data. Hence, the injection of the same dose of [^{11}C]DTBZ at 20 min appeared twice as high relative to the [^{11}C]FMZ in the early frames.
177x130mm (200 x 200 DPI)

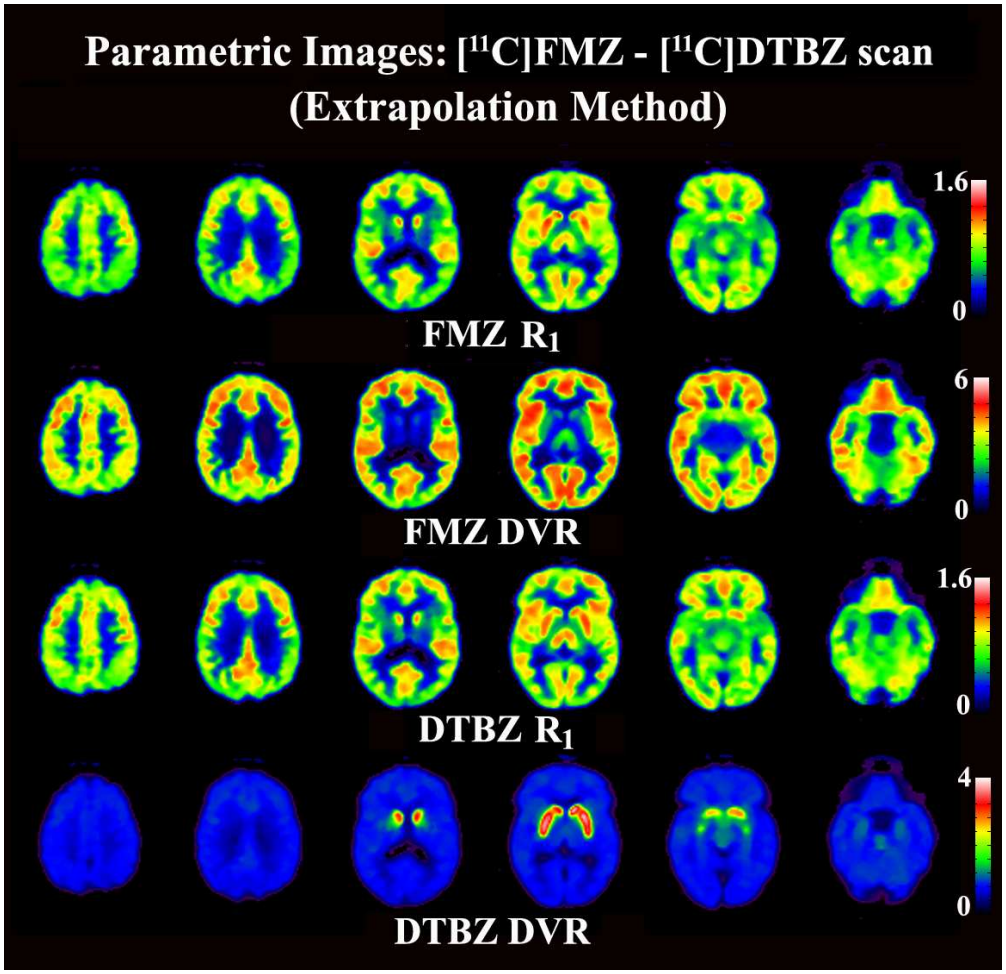

Parametric images obtained from a [^{11}C]FMZ - [^{11}C]DTBZ study at six brain levels.
147x142mm (200 x 200 DPI)

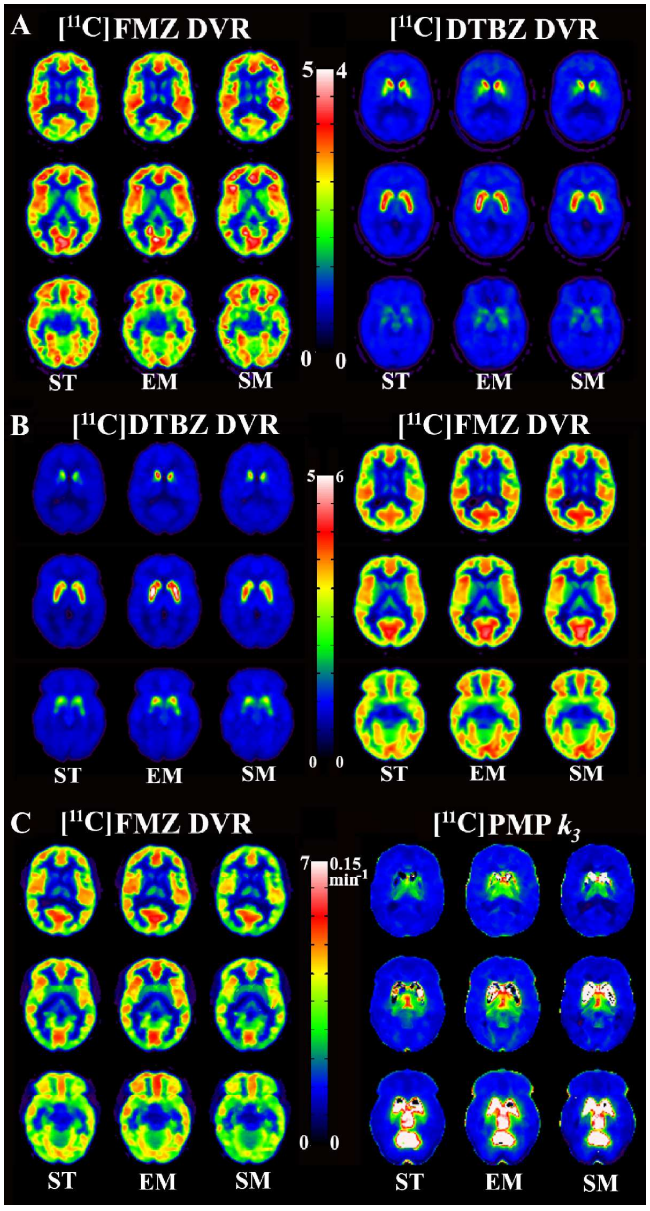

Comparison of parametric images of three brain levels from dual-tracer with those from single-tracer studies. The left-most column for each tracer is from a single-tracer study (ST) which acts as 'gold standard' for comparison of dual tracer results. Panel A: [11C]FMZ injected 20 min prior to [^{11}C]DTBZ. Panel B: [^{11}C]DTBZ injected 30 min prior to [^{11}C]FMZ. Panel C: [^{11}C]FMZ injected 30 min prior to [^{11}C]PMP. The extrapolation method (EM) and simultaneous fitting method (SM) show image patterns and magnitudes very close to those from the single tracer (ST) studies.
152x284mm (400 x 400 DPI)

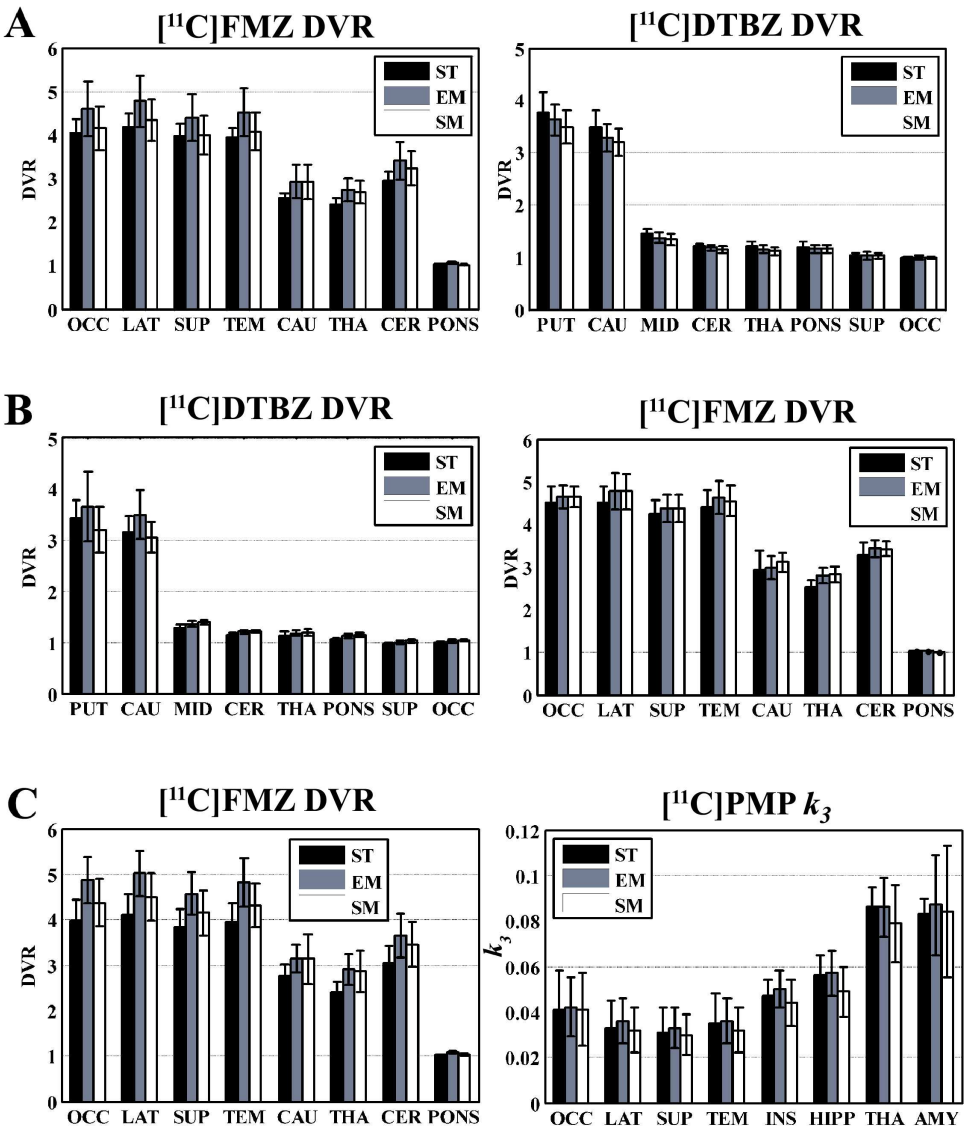

Comparison of inter-subject means and standard deviations in parametric estimates obtained from single-tracer (ST) and dual-tracer studies analyzed using extrapolation method (EM) and simultaneous fitting method (SM). Results from eight regions-of-interest extracted from parametric images are shown. Panel A: Comparison of dual-tracer [^{11}C]FMZ-[^{11}C]DTBZ studies (n=12) with single tracer studies (n=6). Panel B: Comparison of dual-tracer [^{11}C]DTBZ-[^{11}C]FMZ studies (n=6) with single tracer studies (n=3). Panel C: Comparison of dual-tracer [^{11}C]FMZ-[^{11}C]PMP studies (n=19) with single tracer studies (n=10 for [^{11}C]FMZ and n=9 for [^{11}C]PMP). Error bars represent the standard deviation of the estimated parameters. The regions-of-interest for FMZ are: OCC: occipital cortex, LAT: lateral frontal cortex, SUP: superior parietal cortex, TEM: lateral temporal cortex, CAU: caudate nucleus, THA: thalamus, CER: cerebellar hemisphere, PONS: pons. The regions-of-interest for DTBZ are: PUT: putamen, CAU: caudate nucleus, MID: midbrain, CER: cerebral hemisphere, THA: thalamus, PONS: pons, SUP: superior parietal cortex, OCC: occipital cortex. The regions-of-interest for PMP are: OCC: occipital cortex, LAT: lateral frontal cortex, SUP:

superior parietal cortex, TEM: lateral temporal cortex, INS: insular cortex, HIPP: hippocampus, THA: thalamus, AMY: amygdala.
148x175mm (400 x 400 DPI)